Materials Today Bio 16 (2022) 100427

Contents lists available at ScienceDirect

Materials Today Bio

journal homepage: www.journals.elsevier.com/materials-today-bio

Efficient angiogenesis-based wound healing through hydrogel dressing with extracellular vesicles release

Zhengzhe Han [a,1], Lanlan Dong [b,1], Ang Li [a,1], Zongyue Li [c], Landie Fu [d], Zhichang Zhang [a,**], Xiang Li [b,*], Xiaolin Li [a,***]

[a] Department of Orthopedic Surgery, and Shanghai Institute of Microsurgery on Extremities, Shanghai Sixth People's Hospital, 600 Yishan Road, Shanghai, 200233, PR China
[b] School of Mechanical Engineering, Shanghai Jiao Tong University, 800 Dongchuan Road, Shanghai, 200240, PR China
[c] Department of Rehabilitation Medicine, Zhongshan Hospital, Fudan University, 180 Fenglin Road, Shanghai, PR China
[d] North Cross School Shanghai, Building 2, Lane 803, Shuangcheng Road, Baoshan District, Shanghai, PR China

ARTICLE INFO

Keywords:
A. Hydrogel
B. Strength
C. Extracellular vesicles
D. Wound healing dressing

ABSTRACT

Wound healing and angiogenesis remain challenges for both clinical and experimental research worldwide. Periosteum-derived extracellular vesicles (P-sEVs) delivered by hydrogel dressings provide a potential strategy for wound defects to promote fast healing. In this study, we designed a NAGA/GelMA/Laponite/glycerol hydrogel wound dressing that can release P-sEVs to accelerate angiogenesis and wound healing (named P-sEVs@hydrogel) (*N*-acryloyl glycinamide, NAGA). The wound dressing showed multiple functions, including efficient angiogenesis, tissue adhesion and a physical barrier. P-sEVs significantly enhanced the proliferation, migration, and tube formation of endothelial cells *in vitro*. The results of *in vivo* experiments showed that P-sEVs@hydrogel accelerates the healing of a full-thickness defect wound model by stimulating the angiogenic process. The improved cell proliferation, tissue formation, remodeling, and re-epithelialization possibly resulted in the fast healing. This study shows that multifunctional hydrogel dressing combined with bioactive molecules can achieve fast and satisfactory wound healing in full-thickness wound defects and other related wounds.

1. Introduction

Skin is one of the most important and largest organs of the human body [1]. This organ also participates in many essential activities, for example, regulating body temperature, regulating immunity and protecting against water loss [2,3]. Skin defects are a severe condition commonly observed in many traumatic injuries and may cause pain, infection, and other damage to the human body [4,5]. To date, different kinds of wound dressings based on nanomaterials, including foam, electrospun nanofibers, aerogels, sponges, modified gauze and hydrogels, have been developed and applied to healing skin defects [6–8]. Hydrogels are promising wound dressing materials and are widely used in many conditions [9]. These materials could play an important role as a physical barrier against mechanical injuries during the healing process [10].

Given that the wound regenerative process usually takes a long time and the viability of the extracellular vesicles cannot be maintained, the actual results of extracellular therapeutics may be compromised. Therefore, developing a biocompatible nanomaterial that can maintain extracellular vesicle function and their continuous release is urgently needed. Ideal wound dressings should possess multifunctional properties, such as optimizing the function of endothelial cells and fibroblasts [11,12].

During the wound healing process, it is important to promote the reconstruction of new granulation tissue and accelerate the migration of epithelial cells [13]. Designing hydrogel dressings with excellent mechanical stability for long-term use remains a challenge. In this work, a composite hydrogel with outstanding performance named NAGA/GelMA/Laponite/glycerol hydrogel was designed to solve these problems, which may give the wound dressing the desired function [14,15].

As an important bioactive molecule, extracellular vesicles derived

* Corresponding authors.
** Corresponding author.
*** Corresponding author.
E-mail addresses: zzc163mail@163.com (Z. Zhang), xiangliwj@sjtu.edu.cn (X. Li), lixiaolin@sjtu.edu.cn (X. Li).
[1] These authors had equal contributions to the research.

https://doi.org/10.1016/j.mtbio.2022.100427
Received 18 February 2022; Received in revised form 10 September 2022; Accepted 13 September 2022
Available online 24 September 2022

from the periosteum have attracted widespread attention in recent years for their angiogenic ability [16]. P-sEVs have beneficial functions that are similar to those of mesenchymal stem cells (MSCs). Many studies have reported that P-sEVs can effectively promote the healing process of bone defects and have confirmed osteogenic and angiogenic abilities, but few studies have investigated P-sEVs' function in the wound healing process [17–19]. Moreover, compared to MSCs, P-sEVs have advantages such as a low chance of triggering an immune response, high stability, and easy storage [20]. Worldwide, studies have shown the potential usage of extracellular vesicles as a brand new therapy for wound healing [21]. However, extracellular therapeutics still have some issues due to their rapid clearance rate and relatively short half-life *in vivo*.

Herein, a multifunctional hydrogel with long-term mechanical stability was designed and exhibited an efficient angiogenic ability and extracellular vesicle release to promote wound healing [22]. The microscopic morphology, mechanical properties and swelling properties of the composite hydrogel were characterized [23,24]. In addition, the biocompatibility of the P-sEVs@hydrogel was tested by cell compatibility assays *in vitro* [25]. Animal experiments were performed to evaluate the effect of the multifunctional P-sEVs@hydrogel on the wound healing process of rat skin tissue defects [26–28].

2. Materials and methods

2.1. Synthesis of composite hydrogels

The chemical 2-hydroxy-2-methyl-1-phenyl-1-propanone (IRGACURE 1173) was purchased from Sigma Aldrich (St. Louis, USA). Laponite XLG was purchased from BYK (UK). Glycerin (AR, 99%) and gelatin methacryloyl (GelMA) were obtained from Aladdin (Shanghai, China). *N*-acryloyl glycinamide (NAGA) was supplied by Zhengzhou Alfa Chemical Co., Ltd. (Zhengzhou, China).

Hydrogels were synthesized through a simple one-pot method. First, dried GelMA (0.5 g) and NAGA (3 g) were successively dispersed into ultrapure water (7 ml) by magnetic stirring for 30 min at 50 °C. Subsequently, Laponite (0.2 g) and glycerol (3 ml) were added to the above suspension under vigorous stirring for another 1 h. Then, 1173 reagent (0.1% of NAGA) was quickly added under stirring for 15 min. The uniform solution was promptly cast into molds. Polymerization of the hydrogel was preceded by UV light irradiation to obtain the NAGA/GelMA/Laponite/glycerol composite hydrogel. In this work, hydrogel was used as an abbreviation of the NAGA/GelMA/Laponite/glycerol hydrogels. The P-sEV concentration was adjusted to 2 mg/mL, and 50 μL of P-sEVs was dropped into the hydrogel and immediately used for wound healing.

2.2. Scanning electron microscopy (SEM) analysis

The morphologies of the hydrogels were examined using SEM (JSM-5600, JEOL, Tokyo, Japan) operated at a 5 kV acceleration voltage. Before observation, the hydrogels were freeze-dried at −80 °C for 3 days and then sputter coated with Au for 30 s.

2.3. Swelling tests

The equilibrium swelling ratio of the hydrogels was examined in PBS at 37 °C. The swollen hydrogels were removed and weighed (Wwet) after the excess water on the surface was removed. The hydrogels were then washed with DW, freeze-dried, and then reweighed (Wdry). The equilibrium swelling ratio was calculated as follows:

$$\text{Swelling ratio} = \frac{W_{wet} - W_{dry}}{W_{dry}} \times 100\%$$

2.4. Mechanical testing

For evaluation of the mechanical properties of the hydrogels, a dynamic thermomechanical mechanical analyzer (DMA850, TA Instruments, US) was used to measure the tensile properties of the hydrogels. The crosslinked samples (thickness: 1 mm; width: 5 mm; length: 25 mm) were used for the tensile measurements.

2.5. P-sEVs characterization

The morphology of the obtained P-sEVs was determined by TEM (transmission electron microscope), and 15 μL of the P-sEV suspension was dropped onto copper grids covered with a carbon support film (Zhongjingkeyi Technology, China). The samples were air-dried for 1 min at room temperature, and then, excess fluid was removed with filter paper. The samples were negatively stained with 2% uranyl acetate for 1 min. After that, the stained samples were baked under a lamp for 10 min. Finally, TEM (FEI, USA) was performed at 200 kV to visualize and examine the morphology of the P-sEVs.

The particle size and concentration of P-sEVs were measured using nanoparticle tracking analysis (NTA) at VivaCell Shanghai with ZetaView PMX 110 (Particle Metrix, Meerbusch, Germany) and corresponding software ZetaView 8.04.02. Isolated P-sEV samples were appropriately diluted using 1X PBS buffer (Biological Industries, Israel) to measure the particle size and concentration. NTA measurements were recorded and analyzed at 11 positions. The ZetaView system was calibrated using 110 nm polystyrene particles. The temperature was maintained at approximately 23 °C.

2.6. Biocompatibility test

For determination of whether the P-sEVs@hydrogel could affect endothelial cells *in vitro*, cell proliferation, migration, tube formation, and Live/Dead assays were performed after coculture with hydrogel wound dressing (set as the hydrogel and P-sEVs@hydrogel groups). Cells cultured with DMEM/high glucose culture medium (Cytiva, China) were used as the control group. In this study, human umbilical vein endothelial cells (HUVECs) and human foreskin fibroblasts (HFF-1) were chosen to assess the cytotoxicity of the P-sEVs@hydrogel by Cell Counting Kit-8 (CCK-8) assays according to the manufacturer's instructions. A CCK-8 assay was used to assess HUVEC and HFF-1 proliferation within 5 days of culture time, and the 450 nm absorbance was recorded separately at 1, 3 and 5 days. After 5 days of incubation, the cells in the experimental groups were washed with PBS and stained with Live/Dead (Beyotime, China) to demonstrate the biocompatibility of each group. Transwell assay filters (8-μm pore size, Corning, USA) were used to assess migration. Then, 500 μl of Matrigel and a 24-well plate were used to detect the tube formation activity of the HUVECs, and the results were assessed by counting the tubule number in the network under the microscope (100 ×) after incubation for 6 h and 8 h.

2.7. RNA isolation and RT-qPCR analysis

VEGF and FGF1 gene expression in HUVECs and HFF-1 cells separately was measured on day 7 by a real-time quantitative reverse transcription-polymerase chain reaction (RT–qPCR) system (Bio-Rad, Hercules, CA, USA). Three groups were set as mentioned before. After 7 days of culture, total RNA was extracted from cells and reverse transcribed into complementary DNA (cDNA) using TRIzol reagent (Invitrogen, USA) and a PrimeScript RT reagent kit (TaKaRa Biotechnology, Japan) according to the manufacturer's instructions. Then, diluted cDNA was mixed with the SYBR Green system (GeneCopoeia, USA), forward and reverse primers, and RNase-free water to perform RT–qPCR. The relative quantification of target genes (VEGF and FGF1) was performed with normalization by GAPDH, and the 2-ΔΔCt method was used to calculate the fold changes. All experiments were performed in

quadruplicate. The primer sequences used in this study are listed in Supplementary Table S2.

2.8. In vivo wound healing assay

For evaluation of the *in vivo* wound healing effect of the P-sEVs@hydrogel, Sprague–Dawley rats (330–350 g) were used for a full-thickness wound defect model. Eighteen female rats were used in this experiment. The hydrogel was disinfected with ultraviolet light for 24 h prior to implantation. The rats were housed in an SPF environment. Before surgery, anesthesia was administered intraperitoneally with 3% pentobarbital sodium at a dosage of 1.0 ml/kg. Defect ranges were marked, and regulated full-thickness skin wounds (diameter = 2.0 cm) were established on the rats by excising the dorsal skin. Then, the wounds were filled with hydrogel with or without P-sEVs. Transparent film dressing was applied to the wound to fix the hydrogel so it would remain in place. After surgery, every rat received an antibiotic such as penicillin injection. The penicillin was dissolved in normal saline at a concentration of 800,000 U/ml at a dosage of 80,000 U per rat.

The photos of the rats were taken by a camera on days 0, 3, 7, and 14 post-surgery. The wound margin and range were measured by analysis software (NIH Image). The amount of wound closure was calculated using the following formula:

$$\text{Percent wound area reduction} = [(A_0 - A_t) / A_0]^* 100\%$$

where A_0 is the initial wound area ($t = 0$) and A_t is the wound area at each time point.

The rats were euthanized at 7 and 14 days after surgery. The wound tissues with healthy skin were removed. Formalin was used to fix the samples. The samples were dehydrated and embedded in paraffin. Six-micrometer-thick sections were stained with HE and Masson's trichrome. These sections were observed under a microscope. The newborn epithelium was determined.

Immunofluorescence staining was performed on the sections to determine angiogenesis during wound healing. Immunofluorescence staining was utilized to show CD31 (1:100, shown in red) and α-SMA (1:100, shown in green), which are markers of endothelial cells. Type I collagen (1:100, shown in red) and type III collagen (1:100, shown in green) were also shown with immunofluorescence staining. For immunofluorescence staining, the slides were rehydrated and blocked with 1.5% goat serum (Millipore, US). The primary antibody was incubated at 4 °C overnight. The secondary antibody, fluorescyl-tyramide hydrogen peroxide amplification reagent and diamidinephenylindole-dihydrochloride (DAPI; Sigma–Aldrich, Buchs, Switzerland) were applied. The slides were detected using a fluorescence microscope (DMI6000 B, Leica, Germany).

The quantitation of the vessels was performed and analyzed for different samples in each group using ImageJ software.

2.9. Statistical analysis

The statistical analysis was carried out using Origin Pro 2016 (OriginLab, Berkeley, CA, USA). All data are shown as the mean ± standard deviation (SD).

3. Results and discussion

3.1. Scanning electron microscopy (SEM) analysis

As shown in Fig. 1(A), SEM was used to observe the microscopic morphology of the hydrogel surface. The hydrogel has an interconnected porous microstructure, which is shown in Fig. 1(B). This porous structure is conducive to wound healing. It can promote the transmission of nutrients and cell waste in wound defects and promote cell proliferation.

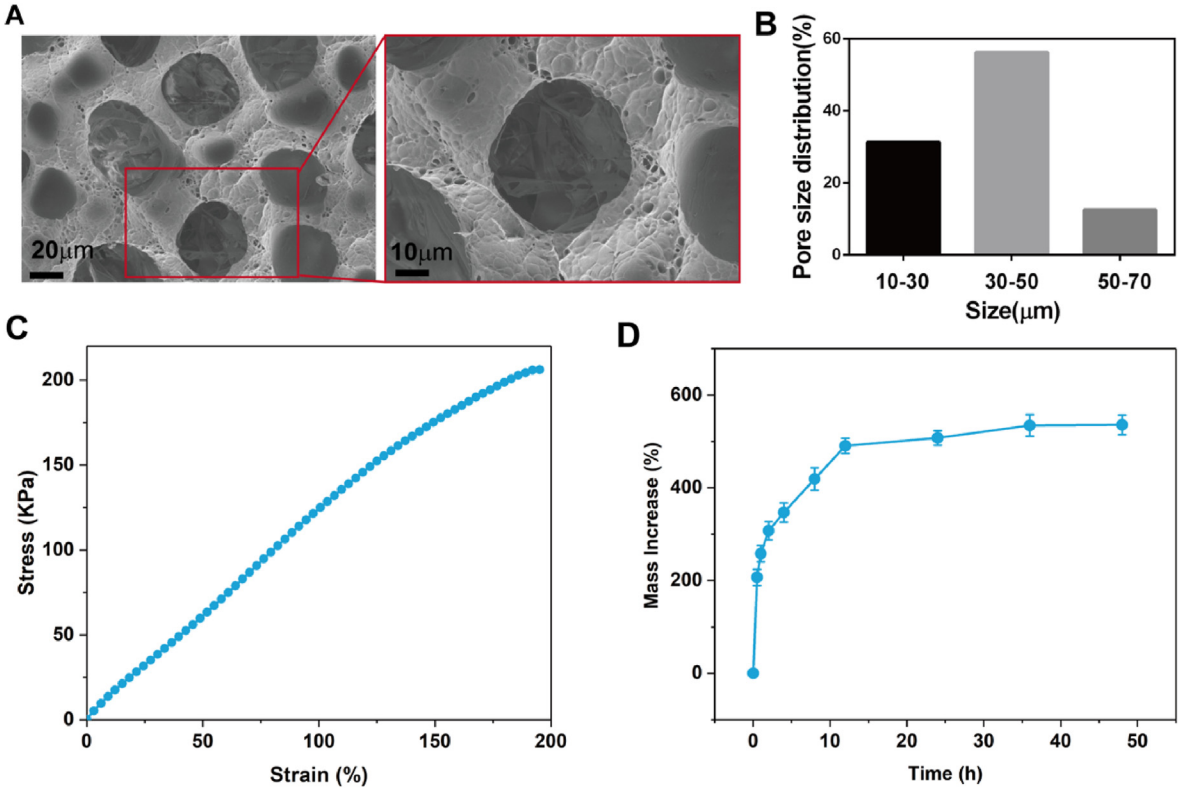

Fig. 1. Characterization of the NAGA/GelMA/Laponite/glycerol hydrogel. (A) SEM images of the hydrogel. (B) The pore size distribution ratio of hydrogels of different sizes. (C) Tensile stress−strain plots of the hydrogel. (D) The swelling ratio of the hydrogel.

3.2. Mechanical testing

As shown in Fig. 1(C), the ideal wound dressing should match the modulus of human tissue, so the corresponding Young's modulus and failure strain were calculated through tensile experiments. Importantly, the Young's modulus of the hydrogel (117 ± 14 kPa) is highly matched with the modulus of human skin (within the range of 100 kPa), and the elongation rate (178 ± 19) is higher than the skin elongation rate (approximately 70%) [29,30]. Therefore, hydrogels with good mechanical properties are potential candidates for wound dressings.

3.3. Swelling tests

The swelling behavior of hydrogels is presented in Fig. 1(D). There was an evident increase in the mass during the first 0.5 h. Subsequently, the swelling rate of the hydrogel reached nearly 500% within 12 h. Finally, the obtained hydrogel required more than 24 h to reach equilibrium swelling. This swelling property allows the hydrogel to be used as a carrier for exosome release on the one hand and to absorb the exudate from the wound site on the other hand.

3.4. Characterization of P-sEVs

P-sEVs were isolated from the culture medium of periosteal cells. TEM analysis revealed that both P-sEVs were double-layered vesicles with intact membrane structures and typical cup shapes, as shown in Fig. 2(A). As shown in Fig. 2 (B), the average diameter of P-sEVs was 101.96 nm. The particle size distribution was still in the range of 50–200 nm and met the definition of sEVs.

3.5. In vitro evaluation of biocompatibility and angiogenic activity

To assess whether the P-sEVs@hydrogel could affect endothelial cell behaviors *in vitro*, we evaluated cell proliferation, migration, and tube formation and performed RT–qPCR [31,32], as shown in Fig. 3. The P-sEVs@hydrogel group showed higher cell viability than the control group and the hydrogel group, as shown in Fig. 3(A and B), indicating that extracellular vesicles released from the hydrogel can promote HUVEC and HFF-1 cell proliferation [33,34]. The results shown in Fig. 3(C) show that the relative expression of VEGF in the hydrogel and P-sEVs@hydrogel groups was higher than that in the control group, while VEGF expression in the hydrogel group was higher than that in the P-sEVs@hydrogel group. This result may indicate that both the hydrogel and P-sEVs@hydrogel groups showed enhanced VEGF gene expression in HUVECs. Laponite in the hydrogel could upregulate VEGF gene expression, while the combination of Laponite and P-sEVs may have a more complex effect [35,36]. The results shown in Fig. 3(D) indicate that the relative expression of FGF1 in the hydrogel and P-sEVs@hydrogel groups was higher than that in the hydrogel group, while FGF1 expression in the P-sEVs@hydrogel group was higher than that in the hydrogel group. This result may indicate that the P-sEVs@hydrogel can significantly promote FGF1 gene expression in HFF-1 cells [37–39]. Cell viability was measured by live/dead staining, as shown in Fig. 3(E, F, G). The results were analyzed by NIH Image software. This result may indicate that both the hydrogel and P-sEVs@hydrogel groups possess good biocompatibility. Furthermore, the results of the migration and tube formation assays, which are shown in Fig. 3(J), demonstrated that compared to the control and hydrogel groups, the P-sEVs@hydrogel group showed substantially enhanced motility and *in vitro* angiogenesis of HUVECs. Statistical analysis from Fig. 3(H) and (I) presents the migration results after 48 h along with the tube formation results after 6 and 8 h, both of which suggest that the hydrogel dressing has outstanding biocompatibility and that the P-sEVs released from the P-sEVs@hydrogel can activate multiple angiogenic behaviors of HUVECs, such as cell proliferation, migration and tube formation *in vitro,* identifying a potential strategy in clinical wound healing. Further studies are needed to test the effect of the P-sEVs@hydrogel at the gene level [40,41]. Although the effect of P-sEVs@hydrogel on the VEGF gene expression of HUVECs was less obvious than that of the hydrogel group, considering the comprehensive effect on cell proliferation, migration, and tube formation effects on HUVECs, along with the direct outcomes of *in vivo* experiments, we still believe the P-sEVs@hydrogel group possesses better biocompatibility and angiogenic activity than the hydrogel group.

3.6. In vivo wound healing in a full-thickness skin defect model

The above results prove that the P-sEVs@hydrogel has multifunctional properties and good biocompatibility together with a strong angiogenic ability, which should be favorable for wound healing [42,43]. We evaluated the wound healing ability of the P-sEVs@hydrogel dressing using a full-thickness wound defect model. Fig. 4(A) shows gross images of wounds at different time points (0, 3, 7 and 14 days). After 14 days of treatment, the wound areas of all groups were significantly reduced, while the P-sEVs@hydrogel group showed the fastest healing (Fig. 4(B)). Compared with those in the control and hydrogel groups, the wounds in the P-sEVs@hydrogel group showed the best healing 14 days later, with newly formed skin observed [44]. However, the wounds in the control group were still exposed and covered with scars, while the hydrogel group showed better healing results than the control group. The wound margin and range were measured by analytical software (NIH Image). The amount of wound closure was calculated using the following formula:

$$\text{Wound area ratio } (\%) = \frac{A_0 - A_t}{A_0} \times 100$$

where A_0 is the initial wound area (t = 0) and A_t is the wound area at each time point.

The wound closure rate also confirmed the gross observation results (Fig. 4(C)). At day 3, which is the very early healing period, the P-

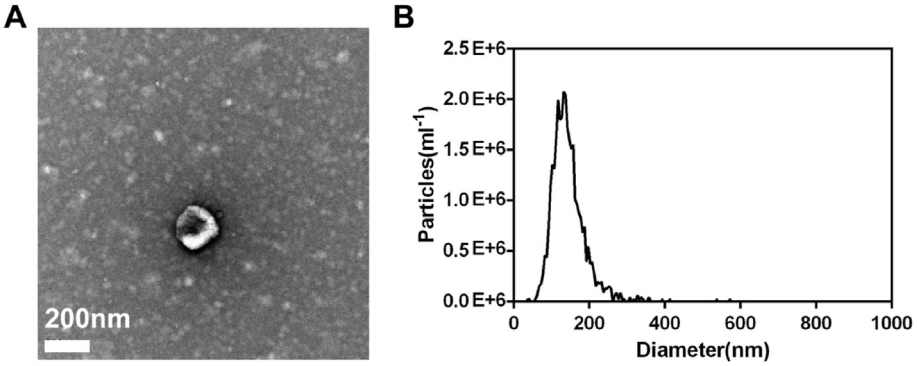

Fig. 2. Characterization of P-sEVs. (A) TEM images of P-sEVs (scale bar = 200 nm). (B) Particle size distribution of P-sEVs.

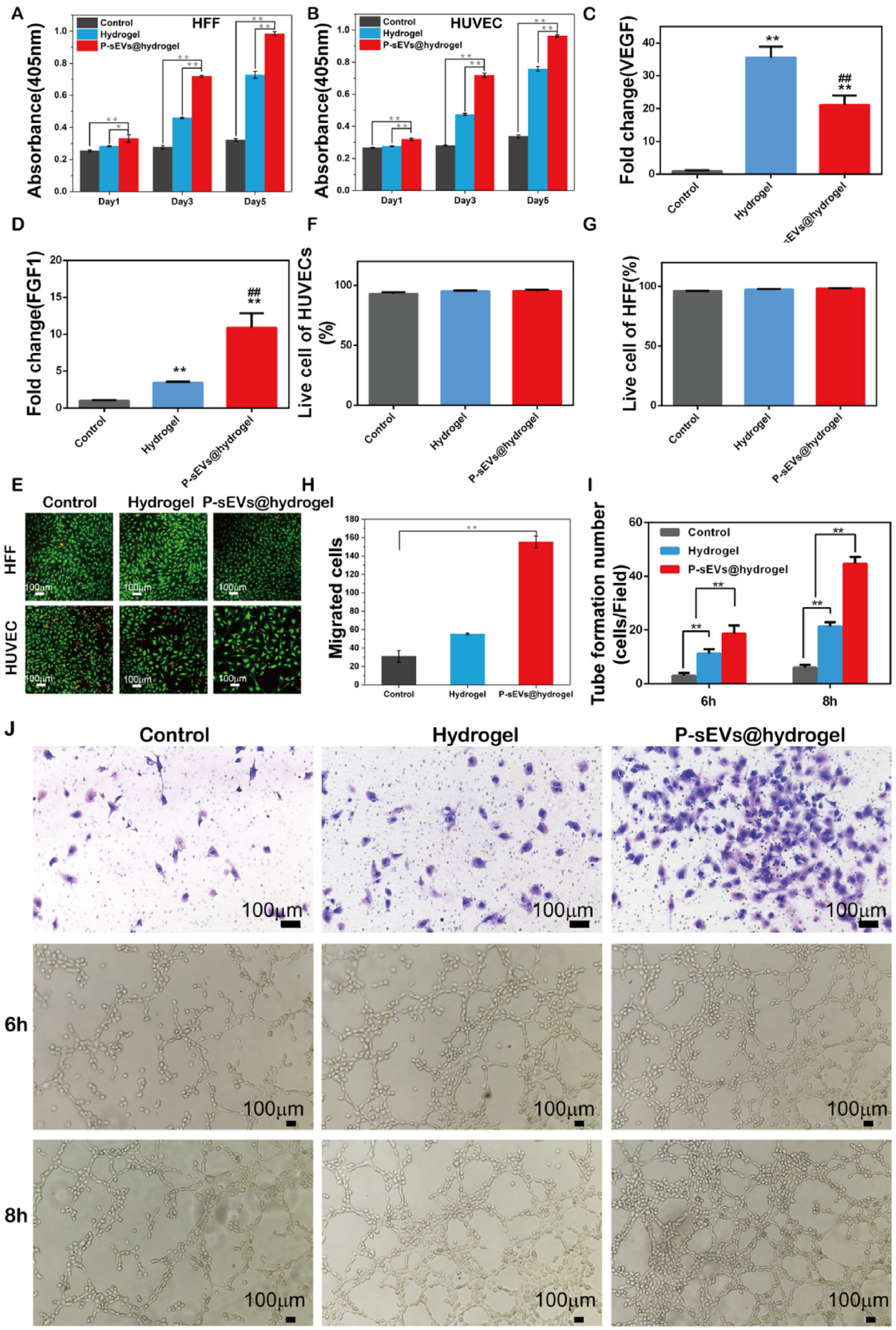

Fig. 3. Wound healing capability of the control/hydrogel/P-sEVs@hydrogel group *In vitro*. Cytocompatibility of HFF-1 cells (A) and HUVECs (B). (C) Relative expression of VEGF in HUVECs in the control/hydrogel/P-sEVs@hydrogel group. (D) Relative expression of FGF1 in HFF-1 cells in the control/hydrogel/P-sEVs@hydrogel group. (E) Live/Dead staining images of the control/hydrogel/P-sEVs@hydrogel group after 5 days of coculture with HUVECs and HFF-1 cells (scale bar = 100 μm). (F, G) Live cell percentage of HUVECs and HFF-1 cells in the control/hydrogel/P-sEVs@hydrogel group. (H, I, J) Transwell results after 48 h coculture (scale bar = 100 μm) and tube formation results after 6 and 8 h coculture (scale bar = 100 μm).

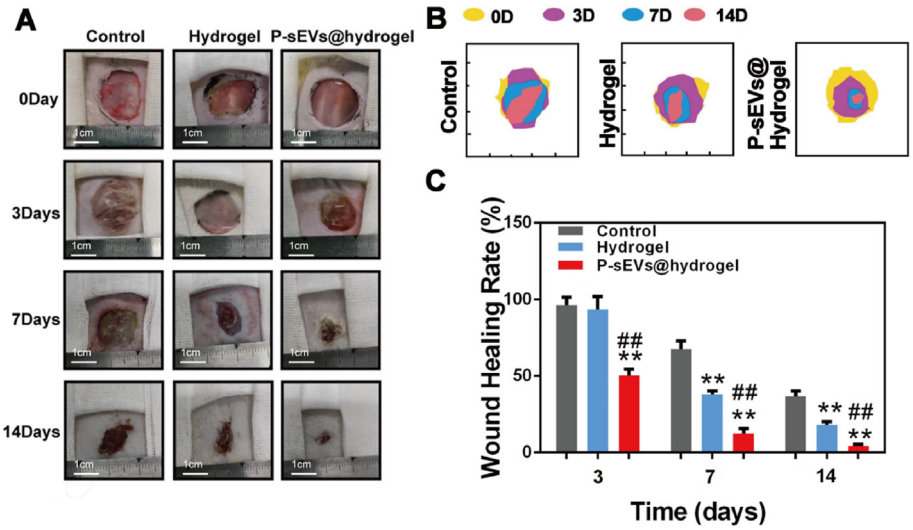

Fig. 4. Wound healing capability of the control/hydrogel/P-sEVs@hydrogel group *in vivo*. (A) Gross images of a representative rat from each group were taken post-implantation on days 0, 3, 7, and 14 (scale bar = 1 cm). (B) Wound area of each group at different time points. (C) Quantification of wound closure rate.

sEVs@hydrogel group showed a significantly higher healing rate than the control and hydrogel groups. After day 7, the P-sEVs@hydrogel showed the highest healing rate among the groups, followed by the hydrogel group. The results indicate that P-sEVs loaded in hydrogel can not only maintain their function *in vitro* but also play a crucial role in the regeneration of skin defects *in vivo*.

3.7. Histological evaluation of regenerated tissues

H&E and Masson's trichrome staining of wound samples were used to assess the histological status during the healing period of 7 and 14 days (Fig. 5(A)). On the 7th day, no obvious epidermal defects were observed in the P-sEVs@hydrogel group compared with the control and hydrogel groups, which indicates a good trend of wound healing. On the 14th day, the wounds in all groups healed generally and were covered with neo-epidermis. However, the thickness, differentiation status and wound length of each group were obviously different. The shortest wound length appeared in the P-sEVs@hydrogel group, while the other groups had a longer wound area (Fig. 5(B)). The H&E staining results indicate that wounds treated with the P-sEVs@hydrogel can achieve more satisfying healing with not only a faster healing rate but also more skin appendages in the scar area. Moreover, Masson staining showed collagen deposition in the wounds in different groups, and the greatest collagen-positive area was observed in the P-sEVs@hydrogel group (Fig. 5(C)). Newly formed collagen in all groups increased on the 7th and 14th days. However, the collagen fibers in the P-sEVs@hydrogel were more organized than those in the control and hydrogel groups. Skin appendages observed in the P-sEVs@hydrogel group also confirmed the results of H&E staining. Combined with the results of H&E staining and Masson staining, these findings indicated that the wounds treated with P-sEVs@hydrogel showed an effectively enhanced re-epithelialization process.

3.8. Expression of CD31, α-SMA, collagen I and collagen III during the wound healing process

CD31, α-SMA, collagen I and collagen III are common indicators of skin formation [45,46]. Therefore, immunostaining of such indicators was used to evaluate the amount of blood vessels, fibroblasts and myofibroblasts in different groups (Fig. 6). CD31 immunostaining was performed on tissue slice samples to determine the influence of each treatment on blood vessel formation [47,48]. Immunostaining for α-smooth muscle actin (α-SMA) indicated mature blood vessels (Fig. 6(A)). As shown in Fig. 6(A), on the 7th day, the control group and the hydrogel group had a small amount of blood vessel formation; however, the P-sEVs@hydrogel group had a larger amount of blood vessel formation, and the number of blood vessels was significantly greater than that in the other groups (Fig. 6(B)). On the 14th day, the number of blood vessels decreased in all groups because the wounds in the later stage of healing needed fewer blood vessels for remodeling, and the blood vessels became mature (Fig. 6(C)). The expression levels of collagen I and collagen III reflect collagen activation and deposition during wound healing [49]. As shown in Fig. 6(A), strong positive staining of both types (collagen I and III) was observed in all groups on the 7th day, while the P-sEVs@hydrogel group showed the most obvious staining. On the 14th day, the collagens in all groups increased compared to those the 7th day; nevertheless, a significantly higher staining level was found in the P-sEVs@hydrogel group, followed by the hydrogel group. The immunostaining results confirmed that the P-sEVs@hydrogel group showed more granulation tissue and collagen deposition during the wound healing process.

4. Conclusion

In this study, we fabricated an angiogenic hydrogel wound dressing with therapeutic extracellular vesicle release to promote wound healing. P-sEVs are used to treat bone defects, but they were used here in the wound healing process for the first time, and the results have proven their efficiency and potency in clinical application. P-sEVs were derived from periosteal cells, which have been proven to have outstanding biocompatibility. Combined with NAGA/GelMA/Laponite/glycerol hydrogel, a new wound dressing with a good angiogenic ability was fabricated. The P-sEVs@hydrogel dressing enhanced the proliferation, migration and tube formation of HUVECs. The P-sEVs@hydrogel dressing could also promote proliferation and angiogenesis in regenerated tissue, which resulted in faster granulation tissue formation, collagen deposition and remodeling, accelerated wound healing and regenerated skin appendages in healed wounds. Extracellular vesicles derived from periosteal cells contain mRNA, miRNA, growth factors and other kinds of proteins that can be transferred to target cells to mediate intercellular communication and biological wound healing processes, which provide a new strategy in wound healing. The effect of extracellular vesicles is transient and difficult to sustain for a long period of time, but our *in vitro*

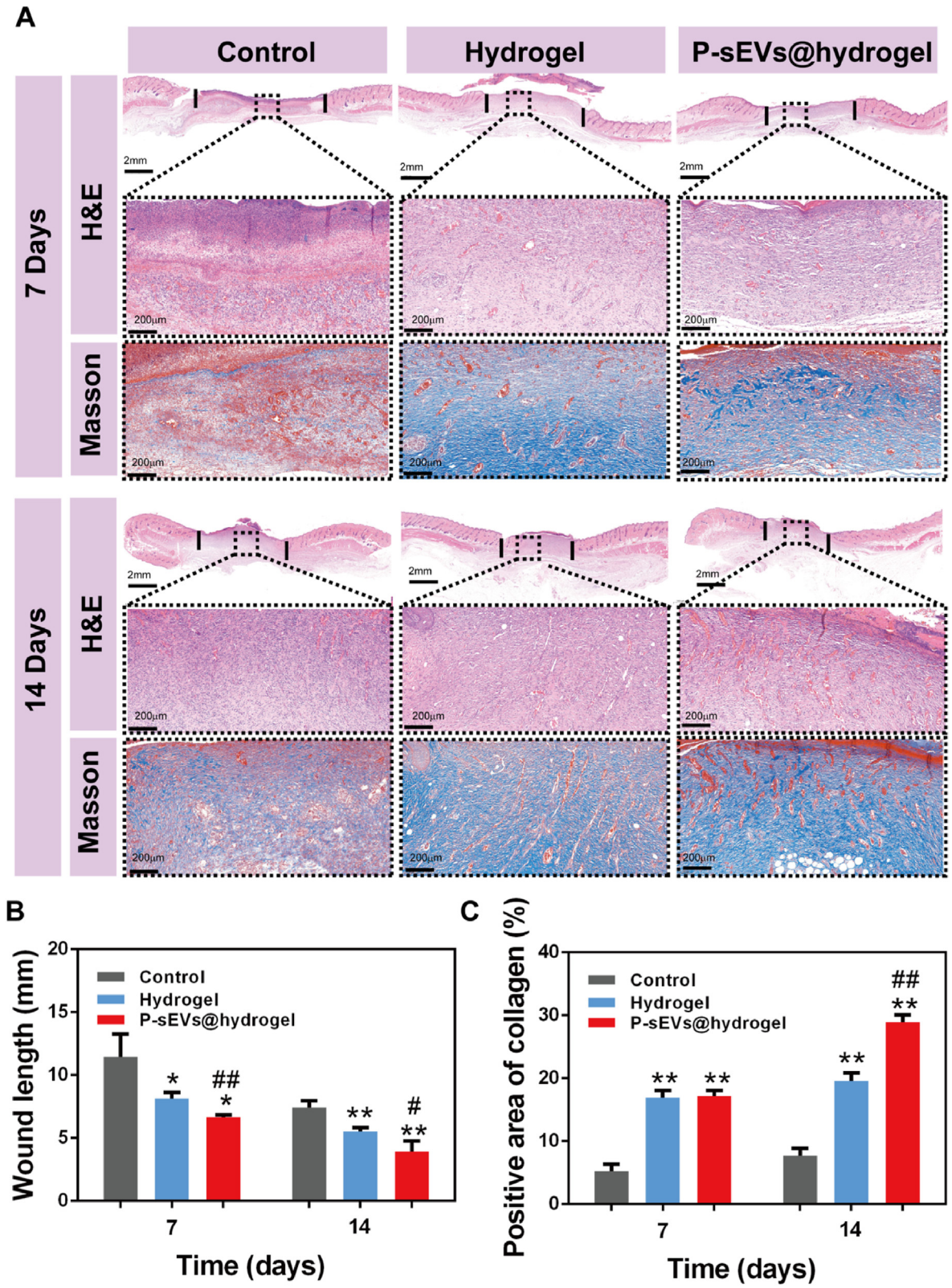

Fig. 5. Histological evaluation of regenerated tissues. (A) Images of H&E staining and Masson's trichrome staining of the wound tissues treated with the control, hydrogel, and P-sEVs@hydrogel for 7 and 14 days (scale bar = 200 μm). (B) Quantification of the wound length in the tissues on days 7 and 14. (C) Quantification of the positive area of collagen in the wound tissues on days 7 and 14.

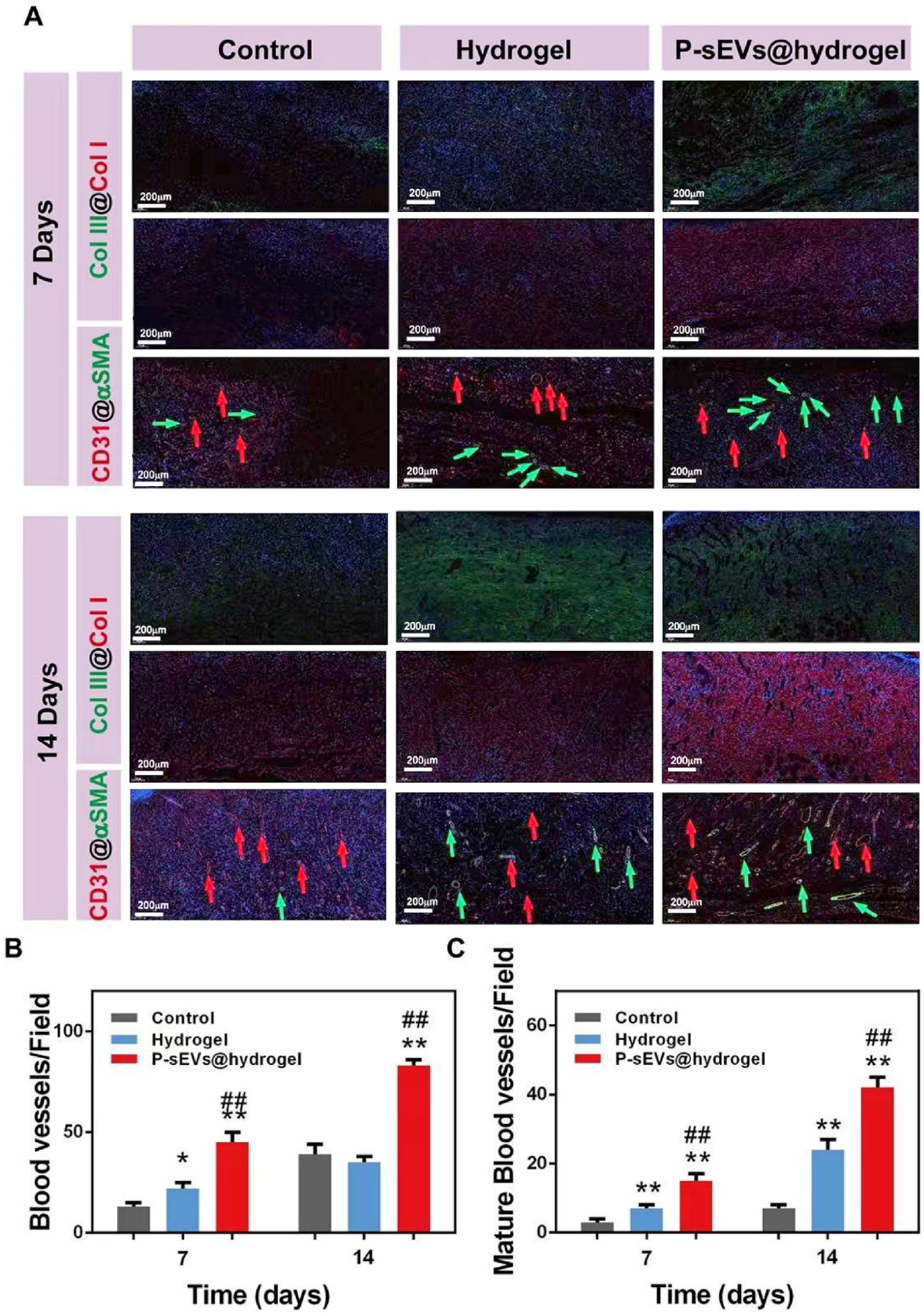

Fig. 6. (A) Immunostaining of collagen I, collagen III, CD31 and α-SMA after 7 and 14 days of treatment (scale bar = 200 μm). (B) Quantitative analysis of blood vessels of groups following different treatments for 7 and 14 days. (C) Quantitative analysis of mature blood vessels following different treatments for 7 and 14 days.

and *in vivo* experiments confirmed the sustained effect of the P-sEVs@hydrogel, which indicated that the hydrogel may slow the release of extracellular vesicles. This study indicates that the P-sEVs@hydrogel could synergistically stimulate angiogenesis in wounds and promote wound healing and skin reconstruction.

Credit author statement

Conceptualization: Zhengzhe Han, Lanlan Dong, Ang Li, Zongyue Li, Landie Fu; Data curation: Zhengzhe Han, Lanlan Dong, Ang Li, Zongyue Li, Landie Fu; Funding acquisition: Zhichang Zhang, Xiang Li, Xiaolin Li; Investigation: Zhengzhe Han, Lanlan Dong, Ang Li, Zongyue Li, Landie Fu; Methodology: Zhengzhe Han, Lanlan Dong, Ang Li; Project administration: Zhengzhe Han, Lanlan Dong, Ang Li; Resources: Zhichang Zhang, Xiang Li, Xiaolin Li; Software: Zhengzhe Han, Lanlan Dong, Ang Li, Zongyue Li, Landie Fu; Writing – original draft writing: Zhengzhe Han, Lanlan Dong; Writing review: Zhichang Zhang, Xiang Li, Xiaolin Li.

Funding

The research received support from the National Natural Science Foundation of China (No.82072422, 81572178, 52075324), Science and Technology Commission of Shanghai Municipality (No. 2020PJD042).

Declaration of competing interest

The authors declare that they have no known competing financial interests or personal relationships that could have appeared to influence the work reported in this paper.

Data availability

Data will be made available on request.

Acknowledgments

The authors thank for the help from Dr. Jinghuan Huang from Department of Orthopedic Surgery, and Shanghai Institute of Microsurgery on Extremities, Shanghai Jiao Tong University Affiliated Sixth People's Hospital.

Appendix A. Supplementary data

Supplementary data to this article can be found online at https://doi.org/10.1016/j.mtbio.2022.100427.

References

[1] D.G. Armstrong, A.J.M. Boulton, S.A. Bus, N. Engl. J. Med. 376 (2017) 2367.
[2] B. Saleh, H. Kaur Dhaliwal, R. Portillo-Lara, E. Shirzaei Sani, R. Abdi, M.M. Amiji, N. Annabi, B. Saleh, R. Portillo Lara, H.K. Dhaliwal, M.M. Amiji, R. Portillo-Lara, E. Shirzaei Sani, N. Annabi, R. Abdi, Small 15 (2019), 1902232.
[3] R.E. Jones, D.S. Foster, M.T. Longaker, JAMA, J. Am. Med. Assoc. 320 (2018) 1481.
[4] R. Zeng, C. Lin, Z. Lin, H. Chen, W. Lu, C. Lin, H. Li, Cell Tissue Res. 374 (2018) 217.
[5] A.J. Rosenbaum, S. Banerjee, K.M. Rezak, R.L. Uhl, J. Am. Acad. Orthop. Surg. 26 (2018) 833.
[6] S. Li, A. Chen, Y. Chen, Y. Yang, Q. Zhang, S. Luo, M. Ye, Y. Zhou, Y. An, W. Huang, T. Xuan, Y. Pan, X. Xuan, H. He, J. Wu, Chem. Eng. J. 402 (2020), 126202.
[7] H. Lu, Q. Wang, G. Li, Y. Qiu, Q. Wei, Mater. Sci. Eng. C 74 (2017) 86.
[8] S. Manchineella, G. Thrivikraman, K.K. Khanum, P.C. Ramamurthy, B. Basu, T. Govindaraju, Adv Healthc Mater 5 (2016) 1222.
[9] F.Y. Han, K.J. Thurecht, A.K. Whittaker, M.T. Smith, Front. Pharmacol. 7 (2016), https://doi.org/10.3389/FPHAR.2016.00185.
[10] Y. Hu, Z. Zhang, Y. Li, X. Ding, D. Li, C. Shen, F.-J. Xu, Y. Hu, Z. Zhang, Y. Li, X. Ding, F. Xu, D. Li, C. Shen, Macromol. Rapid Commun. 39 (2018), 1800069.
[11] M. Li, J. Chen, M. Shi, H. Zhang, P.X. Ma, B. Guo, Chem. Eng. J. 375 (2019), 121999.
[12] Q. Chen, H. Chen, L. Zhu, J. Zheng, Macromol. Chem. Phys. 217 (2016) 1022.
[13] Q. Chen, L. Zhu, H. Chen, H. Yan, L. Huang, J. Yang, J. Zheng, Adv. Funct. Mater. 25 (2015) 1598.
[14] Z. Feng, H. Zuo, W. Gao, N. Ning, M. Tian, L.Z. Zhang Feng, H. Zuo, W. Gao, N. Ning, M. Tian, L. Zhang, Macromol. Rapid Commun. 39 (2018), 1800138.
[15] Y.J. Wang, C.Y. Li, Z.J. Wang, Y. Zhao, L. Chen, Z.L. Wu, Q. Zheng, J. Polym. Sci. B Polym. Phys. 56 (2018) 1281.
[16] S. Debnath, A.R. Yallowitz, J. McCormick, S. Lalani, T. Zhang, R. Xu, N. Li, Y. Liu, Y.S. Yang, M. Eiseman, J.H. Shim, M. Hameed, J.H. Healey, M.P. Bostrom, D.A. Landau, M.B. Greenblatt, Nature 562 (2018) 7725, 2018, 562, 133.
[17] L. Ortinau, K. Lei, Y. Jeong, D. Park, JoVE 2020 (2020) 1.
[18] L. Deveza, L. Ortinau, K. Lei, D. Park, PLoS One 13 (2018), https://doi.org/10.1371/journal.pone.0190909.
[19] L.C. Ortinau, H. Wang, K. Lei, L. Deveza, Y. Jeong, Y. Hara, I. Grafe, S.B. Rosenfeld, D. Lee, B. Lee, D.T. Scadden, D. Park, Cell Stem Cell 25 (2019) 784.
[20] M.A. Serowoky, C.E. Arata, J.G. Crump, F.v. Mariani, Development (Camb.) (2020) 147, https://doi.org/10.1242/dev.179325.
[21] T. H. Ambrosi, C. K. F. Chan, 2021, 1.
[22] J. Yang, V. Cristian, A. Dong, J. Zhang, Macromol. Chem. Phys. (2021) 222, https://doi.org/10.1002/MACP.202000429.
[23] X. Zhao, P. Li, B. Guo, P.X. Ma, Acta Biomater. 26 (2015) 236.
[24] F. Zhang, H. Yang, Y. Yang, H. Wang, X. Li, X. Wu, Chem. Eng. J. 417 (2021), 129145.
[25] I. Sulaeva, H. Hettegger, A. Bergen, C. Rohrer, M. Kostic, J. Konnerth, T. Rosenau, A. Potthast, Mater. Sci. Eng. C 110 (2020), 110619.
[26] T. Chen, Y. Yang, H. Peng, A.K. Whittaker, Y. Li, Q. Zhao, Y. Wang, S. Zhu, Z. Wang, Carbohydr. Polym. 266 (2021), 118122.
[27] G. Chitra, D.S. Franklin, S. Sudarsan, M. Sakthivel, S. Guhanathan, Polym. Eng. Sci. 58 (2018) 2133.
[28] N. Janpetch, N. Saito, R. Rujiravanit, Carbohydr. Polym. 148 (2016) 335.
[29] S. Song, Z. Liu, M.A. Abubaker, L. Ding, J. Zhang, S. Yang, Z. Fan, Mater. Sci. Eng. C (2021) 126, https://doi.org/10.1016/J.MSEC.2021.112171.
[30] H. Liu, Z. Li, Y. Zhao, Y. Feng, A.v. Zvyagin, J. Wang, X. Yang, B. Yang, Q. Lin, ACS Appl. Mater. Interfaces 13 (2021), 26770.
[31] P. Zhang, X. Liu, P. Guo, X. Li, Z. He, Z. Li, M.J. Stoddart, S. Grad, W. Tian, D. Chen, X. Zou, Z. Zhou, S. Liu, Bioact. Mater. 6 (2021) 3097.
[32] Y. Peng, D. He, X. Ge, Y. Lu, Y. Chai, Y. Zhang, Z. Mao, G. Luo, J. Deng, Y. Zhang, Bioact. Mater. 6 (2021) 3109.
[33] X. Zhao, H. Wu, B. Guo, R. Dong, Y. Qiu, P.X. Ma, Biomaterials 122 (2017) 34.
[34] S.H. Kim, K. Kim, B.S. Kim, Y.H. An, U.J. Lee, S.H. Lee, S.L. Kim, B.G. Kim, N.S. Hwang, Biomaterials 242 (2020), 119905.
[35] G. Cidonio, C.R. Alcala-Orozco, K.S. Lim, M. Glinka, I. Mutreja, Y.-H. Kim, J.I. Dawson, T.B.F. Woodfield, R.O.C. Oreffo, Biofabrication 11 (2019), 035027.
[36] D.J. Page, C.E. Clarkin, R. Mani, N.A. Khan, J.I. Dawson, N.D. Evans, Acta Biomater. 100 (2019) 378.
[37] L. Dong, Z. Bu, Y. Xiong, H. Zhang, J. Fang, H. Hu, Z. Liu, X. Li, Int. J. Biol. Macromol. 188 (2021) 72.
[38] M.M. Bernal, A. di Pierro, C. Novara, F. Giorgis, B. Mortazavi, G. Saracco, A. Fina, ArXiv (2018), https://doi.org/10.1002/(ISSN)1616-3028.
[39] H.R. Lim, H.S. Kim, R. Qazi, Y.T. Kwon, J.W. Jeong, W.H. Yeo, Adv. Mater. (2020) 32, https://doi.org/10.1002/ADMA.201901924.
[40] M. Liao, P. Wan, J. Wen, M. Gong, X. Wu, Y. Wang, R. Shi, L. Zhang, Adv. Funct. Mater. 27 (2017), https://doi.org/10.1002/ADFM.201703852.
[41] J. Kang, D. Son, G.J.N. Wang, Y. Liu, J. Lopez, Y. Kim, J.Y. Oh, T. Katsumata, J. Mun, Y. Lee, L. Jin, J.B.H. Tok, Z. Bao, Adv. Mater. 30 (2018), https://doi.org/10.1002/ADMA.201706846.
[42] Q. Rong, W. Lei, L. Chen, Y. Yin, J. Zhou, M. Liu, Angew. Chem. Int. Ed. 56 (2017), 14159.
[43] X.P. Morelle, W.R. Illeperuma, K. Tian, R. Bai, Z. Suo, J.J. Vlassak, Adv. Mater. 30 (2018), https://doi.org/10.1002/ADMA.201801541.
[44] Y. Wei, L. Xiang, H. Ou, F. Li, Y. Zhang, Y. Qian, L. Hao, J. Diao, M. Zhang, P. Zhu, Y. Liu, Y. Kuang, G. Chen, Adv. Funct. Mater. 30 (2020), 2005135.
[45] L. Han, K. Liu, M. Wang, K. Wang, L. Fang, H. Chen, J. Zhou, X. Lu, Adv. Funct. Mater. 28 (2018), https://doi.org/10.1002/ADFM.201704195.
[46] S.T. Han, H. Peng, Q. Sun, S. Venkatesh, K.S. Chung, S.C. Lau, Y. Zhou, V.A.L. Roy, Adv. Mater. 29 (2017), https://doi.org/10.1002/ADMA.201700375.
[47] A. Li, Z. Han, Z. Li, J. Li, X. Li, Z. Zhang, Mater. Des. 212 (2021), 110241.
[48] S. Kuroshima, Z. Al-Salihi, J. Yamashita, Clin. Oral Invest. 20 (2016) 727.
[49] A.M.N. Santos, A.P.D. Moreira, C.W.P. Carvalho, R. Luchese, E. Ribeiro, G.B. McGuinness, M.F. Mendes, R.N. Oliveira, Materials 12 (2019), https://doi.org/10.3390/MA12040559.